fluids

MDPI

Article

Optimization of Airflow Field and Experimental Verification for Wheat Cleaning Device Based on CFD-DEM

Chunyan Zhang [1,2], Junrong He [1,2,3], Sai Yang [1], Yinhu Qiao [1,*], Lele Zhou [1] and Leifeng Dai [1]

[1] College of Intelligent Manufacturing, Anhui Science and Technology University, Chuzhou Campus, Chuzhou 239000, China
[2] Anhui Yunlong Grain Machinery Co., Ltd., Fuyang 236500, China
[3] College of Electromechanical Engineering, Liaoyuan Vocational Technical College, Liaoyuan 136200, China
* Correspondence: qyh7926@163.com

Abstract

To address the issues of high impurity rates and grain loss during the wheat cleaning process, a coupled Computational Fluid Dynamics (CFD) and Discrete Element Method (DEM) approach was employed to investigate the internal airflow field and the fluid–solid coupling process of the wheat cleaning device. The numerical simulation of the three-dimensional internal flow field is carried out in the high-Reynolds-number turbulent region, and the transient double precision solver based on the pressure–velocity coupling algorithm is used. The effects of the air inlet velocity and angle on the airflow field distribution and air separation efficiency were analyzed through CFD simulation. Based on this, the structure of the cleaning device was optimized, and the movement characteristics of materials under various wind forces were compared through CFD-DEM coupling simulation. The results showed that the optimal air separation parameters were an air inlet velocity of 10 m/s and an air inlet angle of 20 degrees. Under these conditions, the airflow distribution in the air separation box was uniform, and the impurity separation efficiency reached the highest level. After optimizing the equipment by installing a high-pressure fan, the number of impurities in the wheat collection box under windy conditions was 265, a reduction of 53.8% compared to 573 under windless conditions. Finally, through repeated experiments on the entire machine, it was verified that the impurity rate of the optimized device was 1.722% and the loss rate was 0.622%, which were 0.23% and 0.12% lower than those of the existing equipment, respectively, consistent with the simulation results. This study provides theoretical basis and technical support for the optimization design of wheat cleaning equipment.

Keywords: wheat cleaning device; airflow field; CFD simulation; CFD-DEM coupling; parameter optimization

Academic Editor: Olivier Pironneau

Received: 28 January 2026
Revised: 15 March 2026
Accepted: 22 March 2026
Published: 26 March 2026

1. Introduction

Wheat, as the core crop of China's summer grain production, ranks third globally in terms of its planting area [1]. Its post-harvest cleaning process directly determines the grain's purity, storage safety, and subsequent processing value, serving as one of the key procedures to ensure national food security [2]. Statistics show that the annual grain loss rate caused by the inadequate performance of cleaning equipment in China's wheat cleaning process is approximately 1.5–3%, and the impurity content often exceeds the storage standard (≤2%). This not only results in the waste of grain resources but

also increases the risk of storage mildew and processing energy consumption [3,4]. The essence of the cleaning process is the multi-physical field synergy among the airflow field, the motion of wheat grains/impurities, and the screening of vibrating screens: the airflow field separates light impurities such as short stalks and chaff from wheat grains through drag force, while the vibrating screen promotes grain screen penetration via mechanical vibration, and the coupling effect of the two directly determines the cleaning performance [5]. However, current wheat cleaning equipment generally faces two major technical bottlenecks: first, uneven airflow field distribution and improper matching between wind speed and air inlet angle lead to incomplete separation of light impurities or grain blow-off; second, the fluid–solid coupling mechanism of "airflow–particles–vibration" has not been fully understood, making it difficult to simultaneously reduce both the impurity content and loss rate through single-parameter optimization [6,7]. These two issues have become core obstacles restricting the upgrading of cleaning equipment to possess high precision and high efficiency.

In the field of cleaning airflow field research, Computational Fluid Dynamics (CFD) technology has become the mainstream tool for analyzing flow field characteristics. U Yuko et al. quantified the turbulent characteristics of airflow in the cleaning chamber using Particle Image Velocimetry (PIV), finding that wall friction and internal friction within particle swarms are the main causes of airflow energy attenuation, which provides a theoretical basis for flow channel drag reduction design [8]. Gebrehiwot et al. compared the flow field distribution of three centrifugal fans based on CFD simulation, confirming that adding a cross-flow opening at the fan outlet can improve the airflow uniformity by 15–20% [9]. Domestic studies also focus on airflow parameter optimization: Wang Peng et al. reconstructed the flow field of the cleaning device via CFD, increasing the average wind speed on the screen surface by 2 m/s and reducing the wheat loss rate to 0.89% [10]; aiming at the single air duct defect of the longitudinal axial flow cleaning device, Shen Qiang proposed a dual-duct six-outlet structure, effectively solving the flow field stability problem under high feed rate [11]. Nevertheless, existing studies still have obvious limitations: most only focus on the independent effects of a single wind speed or air inlet angle, failing to conduct parameter coupling optimization combined with the physical properties of wheat grains and short stalks [12]; in addition, some simulation results remain at the numerical level without verifying the actual separation effect of the airflow field through particle motion feedback, resulting in the limited engineering applicability of the optimized parameters.

With the development of multi-physical field simulation technology, CFD-DEM coupling technology has provided a new approach for understanding the fluid–solid coupling mechanism [13]. This technology simulates the airflow field through CFD and describes particle motion via DEM, realizing the two-way data interaction between the gas and solid phases: the airflow exerts drag and lift forces on the particles, while the particle motion feedback affects the airflow distribution through the volume fraction [14]. Lei et al. simulated the motion of rapeseed and wheat in the feeding device using CFD-DEM, confirming that this technology can accurately capture the dynamic coupling relationship between the particle force and airflow field with a prediction error of less than 5% [15]; Chu et al. analyzed the gas–solid two-phase flow in a cyclone separator through coupling simulation, clearly presenting the regulation law of the solid load rate on the vortex structure [16]. Xiao Xingxing et al. applied CFD-DEM to simulate the grain cleaning process, realizing the visual analysis of grain motion trajectories and finding that the shear modulus and particles' quantity have significant impacts on simulation efficiency [17]; the research team led by Zhang Keping revealed the characteristics of the vortex flow field in the cleaning

device based on this technology, confirming the synergistic effect that internal vortices drive short stalk separation and external vortices promote grain collection [18].

CFD-DEM coupling technology has been introduced into the study of wheat cleaning mechanisms. However, existing research primarily focuses on flow field distribution in the main cleaning zone or the optimization of individual airflow parameters, often overlooking the impurity deposition phenomenon caused by the decay of kinetic energy as airflow moves toward the sieve tail. Relying solely on the adjustment of operational parameters frequently fails to resolve the inherent trade-off between impurity content and grain loss. To fill this research gap, this study integrates Computational Fluid Dynamics (CFD) with the Discrete Element Method (DEM) to reveal the gas–solid two-phase flow interaction mechanisms within the cleaning chamber, based on which both the structure and parameters of the device are optimized. The specific objectives and primary contributions of this study are as follows.

Research Objectives:

The key objective is to address the challenges of high impurity content and high grain loss in wheat cleaning operations. By exploring the optimal airflow field configuration and incorporating a local compensatory airflow structure, this study aims to maximize the separation efficiency of light impurities while preventing grain blow-out loss.

Key Scientific Contributions:

Analysis of Fluid–Solid Coupling Mechanisms: Utilizing a bidirectional CFD-DEM coupling model, this study quantifies the impact of airflow energy attenuation on particle swarm motion characteristics. It accurately captures the dynamic interaction patterns of materials with different aerodynamic properties within complex flow fields.

Mechanism-Based Structural Optimization and Experimental Validation: Addressing the impurity deposition at the sieve tail revealed in theoretical simulations, an improved scheme is proposed: installing a high-pressure fan at the bottom rear of the device to generate a local vertical compensatory airflow field. This optimization was validated through full-scale physical experiments, achieving a simultaneous and significant reduction in both the impurity content and loss rate. This provides a theoretical foundation and practical reference for the design of similar agricultural material sorting equipment.

2. Structure and Working Principle of Wheat Cleaning Equipment

The wheat cleaning apparatus is a combined air-sieve cleaning system, primarily comprising a feeding system, cleaning execution system, power control system, and support mobility system (Figure 1). The feeding system centres on the inlet, receiving the mixed wheat material for processing. The cleaning execution system incorporates a vibrating screen, fan, negative pressure dust collection box, high-pressure blower, and air filter. The vibrating screen serves as the core component for material separation. The fan and high-pressure blower collaborate to generate a gradient airflow field. The negative pressure dust collection box connects to the fan to capture lightweight dust-like impurities, while the air filter purifies the airflow to prevent secondary contamination. The power control system incorporates variable-speed motors, frequency converters, and air velocity sensors. The variable-speed motors and frequency converters enable the precise adjustment of the vibrating screen's vibration parameters and the fan's air velocity respectively. The air velocity sensors provide real-time feedback on airflow parameters to ensure cleaning stability. The support and mobility system, comprising a frame and wheels, bears the structural load and facilitates the unit's mobile operation. To address practical production requirements, a high-pressure blower has been added beneath the vibrating screen. This directs the airflow to re-blow impurities not fully separated at the screen's tail end back onto the screening surface, preventing their entrainment with wheat grains into the collection

bin. This enhances the cleaning unit's impurity separation efficiency and reduces the wheat's impurity content.

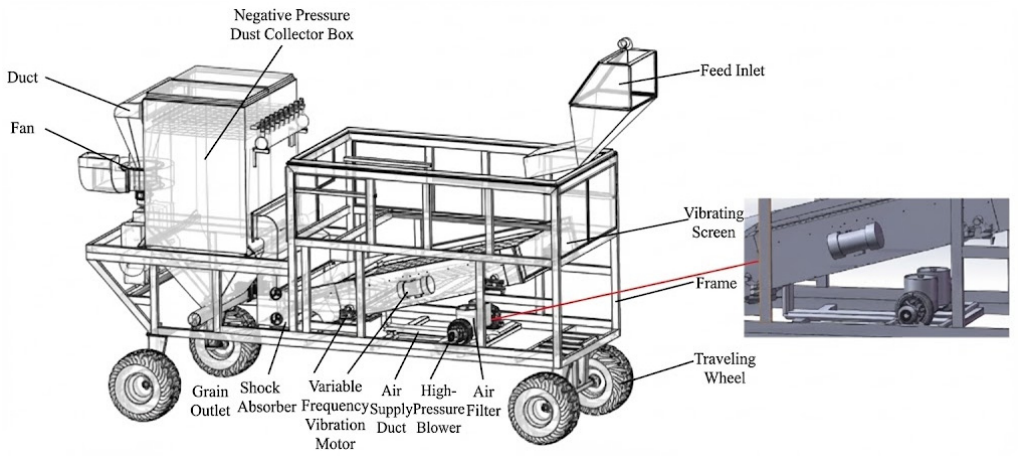

Figure 1. Structure diagram of the wheat cleaning device.

The wheat mixture awaiting cleaning enters the vibrating screen surface through the feed inlet. A variable-speed motor drives the screen to operate according to preset parameters, dispersing the material across the surface whilst imparting directional motion. Concurrently, the fan and high-pressure blower activate, generating a graded airflow field that envelops the screen surface. Leveraging the differences in terminal velocity and particle size between wheat grains and impurities such as short stalks and dust, the vibrating screen separates wheat grains from larger impurities through its mesh openings. The primary airflow field employs drag forces to convey low-suspension-velocity impurities—such as short stalks and lightweight dust—towards the negative-pressure dust collection box for capture. simultaneously purifying the circulating airflow through the air filter. During cleaning operations, should partially cleaned wheat mixtures accumulate at the screen's tail end, the high-pressure blower beneath the vibrating screen adjusts its airflow velocity according to wheat suspension characteristics. This re-blows the impurities back onto the screen surface, preventing their entrainment with wheat grains into the collection bin. Air velocity sensors continuously monitor flow parameters, dynamically adjusting fan speed via a variable frequency drive to maintain airflow stability. Finally, the cleaned wheat kernels are discharged through the outlet, achieving the efficient grading and cleaning of mixed materials.

3. Simulation Analysis and Optimization of Internal Airflow Fields in Cleaning Devices

3.1. Mesh Generation

The fluid domain model was imported into the ANSYS 2022 Version Fluent meshing module, where it was divided using an unstructured triangular mesh. Mesh independence verification was conducted to ensure the simulation's accuracy. The final mesh comprised 2,477,237 elements and 440,089 nodes. The mesh quality was assessed, with an average quality factor exceeding 0.8, meeting the computational requirements. The generated mesh model is illustrated in Figure 2.

Define the walls of the mesh model as the wall, inlet, and outlet according to the boundary conditions. Enable the double-precision solver, proceed to the Fluent settings interface, adopt a transient computational model, and set the gravitational acceleration to 9.81 m/s^2 along the $-$Z direction.

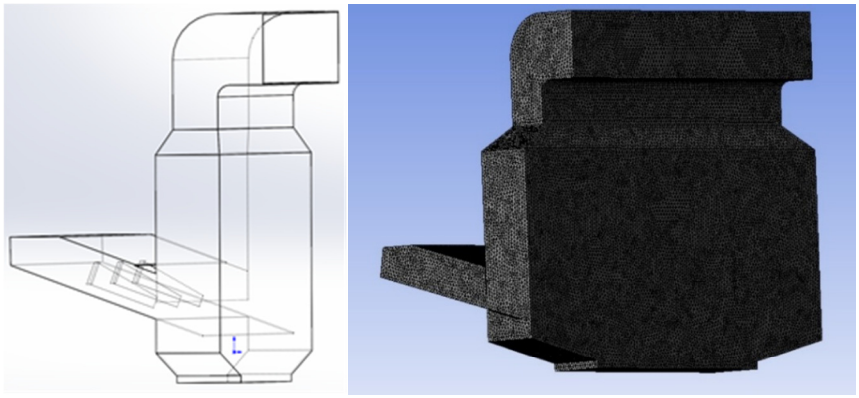

Figure 2. Generating a mesh model.

3.2. Control Equation and Mathematical Model

To accurately describe the movement law of the gas–solid two-phase flow in the wheat cleaning device, this paper adopts the Euler–Lagrange method for the description. Among them, the gas phase (air) is regarded as the continuous phase, and the Navier–Stokes equation is solved by CFD; the wheat and impurity particles are regarded as the discrete phase, their movement trajectories are tracked by DEM, and the two-way coupling calculation is realized through the interphase force. It is assumed that the airflow in the cleaning chamber is an incompressible fluid, and the mass conservation equation and momentum conservation equation are described by tensor symbols, as shown in Equations (1) and (2), respectively:

$$\frac{\partial\left(\alpha_f\rho_f\right)}{\partial t}+\frac{\partial\left(\alpha_f\rho_f u_j\right)}{\partial x_j}=0 \tag{1}$$

$$\frac{\partial\left(\alpha_f\rho_f u_i\right)}{\partial t}+\frac{\partial\left(\alpha_f\rho_f u_i u_j\right)}{\partial x_j}=-\alpha_f\frac{\partial p}{\partial x_i}+\frac{\partial\left(\alpha_f\tau_{ij}\right)}{\partial x_j}+\alpha_f\rho_f g_i+S_{p,i} \tag{2}$$

In the equation, i and j are the tensor indices of the Cartesian coordinate system ($i, j = 1, 2, 3$); α_f is the volume fraction of the fluid; ρ_f is the density of air; u_i u_j is the component of the fluid velocity; p is the fluid pressure; τ_{ij} is the viscous stress tensor; g_i is the component of the gravitational acceleration; and $S_{p,i}$ is the momentum exchange source term between the particles and the airflow.

Given the complex vortex structure in the airflow field within the cleaning device and the relatively high Reynolds number, the standard $k-\epsilon$ turbulence model, which is widely used in engineering and computationally stable, is selected in this paper. This model introduces the transport equations of turbulent kinetic energy k and turbulent kinetic energy dissipation rate ϵ to close the Reynolds-averaged equations, as shown in Equations (3) and (4).

$$\frac{\partial\left(\rho_f k\right)}{\partial t}+\frac{\partial\left(\rho_f k u_j\right)}{\partial x_j}=\frac{\partial}{\partial x_j}\left[\left(\mu+\frac{\mu_t}{\sigma_k}\right)\frac{\partial k}{\partial x_j}\right]+G_k-\rho_f\epsilon \tag{3}$$

$$\frac{\partial\left(\rho_f \epsilon\right)}{\partial t}+\frac{\partial\left(\rho_f \epsilon u_j\right)}{\partial x_j}=\frac{\partial}{\partial x_j}\left[\left(\mu+\frac{\mu_t}{\sigma_\epsilon}\right)\frac{\partial \epsilon}{\partial x_j}\right]+C_{1\epsilon}\frac{\epsilon}{k}G_k-C_{2\epsilon}\rho_f\frac{\epsilon^2}{k} \tag{4}$$

In the equation, G_k refers to the turbulent kinetic energy production term caused by the mean velocity gradient; μ_t represents the turbulent viscosity; $C_{1\epsilon}$, C_j, σ_k, and σ_ϵ denote

the empirical constants of the model. Their values are respectively 1.44, 1.92, 1.0 and 1.3, as specified in the standard turbulence model.

In DEM simulations, wheat kernels and impurities such as short stalks are regarded as discrete elements, whose motion follows Newton's second law. For an arbitrary particle i, its translational and rotational equations are given as follows:

$$m_p \frac{dv_{p,i}}{dt} = F_{drag,i} + F_{g,i} + F_{c,i} + F_{other,i} \quad (5)$$

$$I_p \frac{d\omega_{p,i}}{dt} = T_{c,i} + T_{f,i} \quad (6)$$

In the equations, m_p and I_p represent the particle mass and moment of inertia respectively; $v_{p,i}$ and $\omega_{p,i}$ denote the translational velocity components and angular velocity components of the particle; $F_{g,i}$ stands for gravitational acceleration; $F_{c,i}$ refers to the contact force between particles or between particles and the wall; $T_{c,i}$ represents the contact moment; $T_{f,i}$ is the drag force exerted by the airflow on the particle, and $F_{drag,i}$ is the key force governing the cleaning and separation process.

3.3. Parameter Settings for Boundary Conditions

Considering the terminal velocity characteristics of wheat and impurities alongside the airflow coverage requirements of the cleaning chamber structure, the terminal velocity range for wheat grains is 9.5–10.3 m/s, while impurities such as short stalks and dust exhibit suspension velocities ranging from 2.0 to 6.0 m/s [19], as shown in Table 1. Consequently, a wind speed variable of 5 m/s was selected—below the upper limit of the impurity terminal velocity—to contrast with low-efficiency air separation conditions. This value, approaching the lower limit of wheat terminal velocity at 10 m/s, ensures efficient impurity separation while preventing grain loss. The inlet angle variables of 15°, 20°, and 25° were determined based on the geometric dimensions of the cleaning chamber (length 1900 mm and width 650 mm), as detailed in Table 2. Through a pre-simulation and structural geometric analysis, the influence of different airflow incidence angles on the uniformity of air distribution within the cleaning chamber was investigated.

Table 1. Terminal velocity of wheat rejects.

Different Materials	Terminal Velocity/(m/s)
Wheat grains	9.5~10.3
Husk and light impurities	0.75~5.0
Ears	2.0~5.5
Short stalks	2.0~6.0

Table 2. Multi-factor experimental design.

Factor	Numerical Value
Wind speed (m/s)	5 10
Inlet angle (°)	15 20 25

Boundary conditions are set with air as the fluid medium under standard conditions, possessing a density of 1.205 kg/m^3 and a dynamic viscosity of 1.789 × 10^{-5} Pa·s. The turbulence model employs the standard k-ε model. The inlet is configured as a velocity inlet, while the outlet functions as a pressure outlet with a pressure value of 0 Pa. The solver employs a pressure–velocity coupled algorithm with a transient time history. The maximum

iteration count per time step is set to 500. The simulation's parameters encompass two intake air velocities and three intake angles, yielding a total of six operating conditions.

3.4. Simulation of the Influence of Airflow Parameters on Cleaning Effectiveness

Simulations were conducted for inlet angles of 15°, 20° and 25° at a wind speed of 5 m/s. The simulation results are shown in Figures 3 and 4 below.

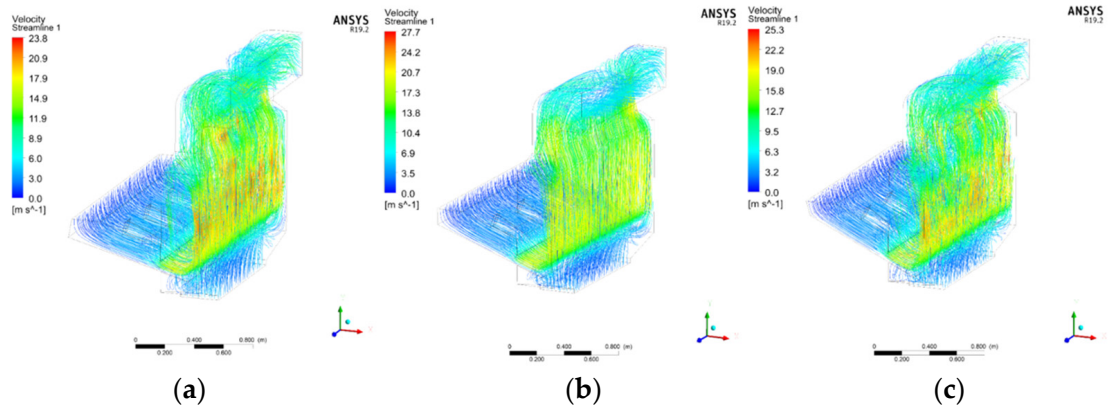

Figure 3. 3D Streamlines of 5 m/s airflow at different inlet angles. (**a**) 15°. (**b**) 20°. (**c**) 25°.

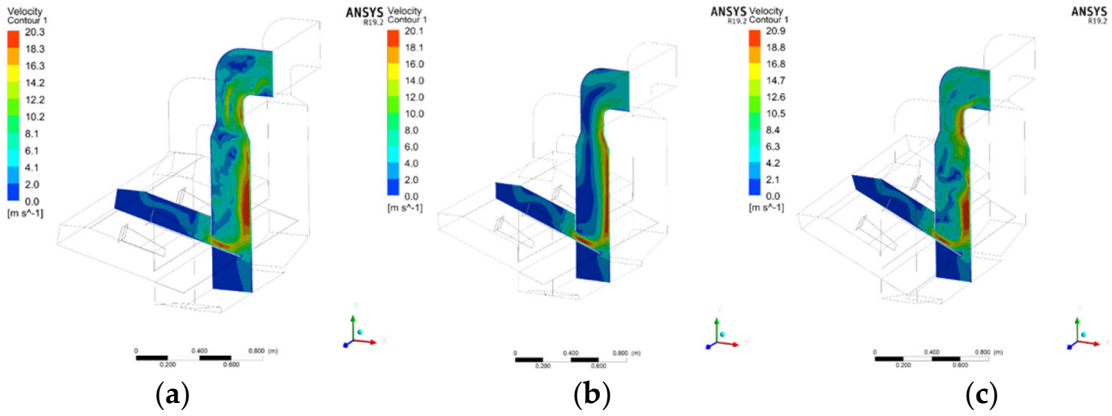

Figure 4. Cloud map of velocity vector at different angles of 5 m/s. (**a**) 15°. (**b**) 20°. (**c**) 25°.

Simulations were conducted for inlet angles of 15°, 20°, and 25° at a wind speed of 10 m/s. The simulation results are shown in Figures 5 and 6 below.

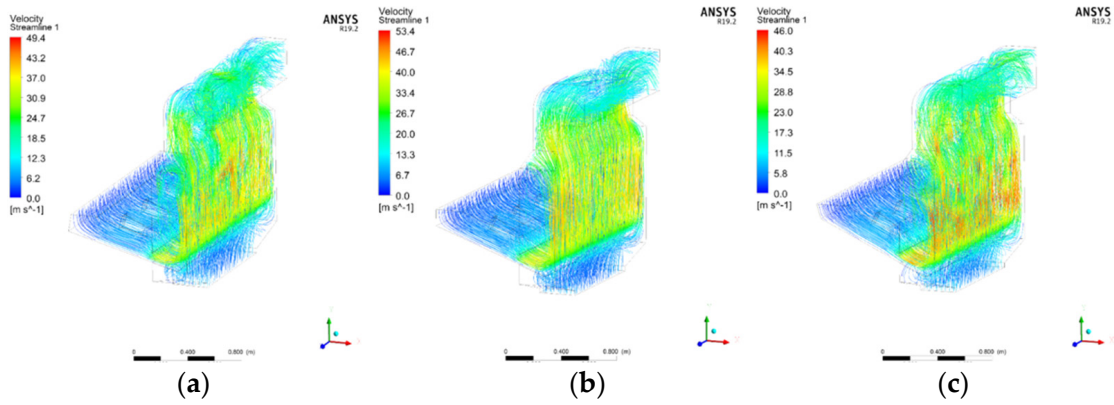

Figure 5. 3D Streamlines of different inlet air angle at 10 m/s. (**a**) 15°. (**b**) 20°. (**c**) 25°.

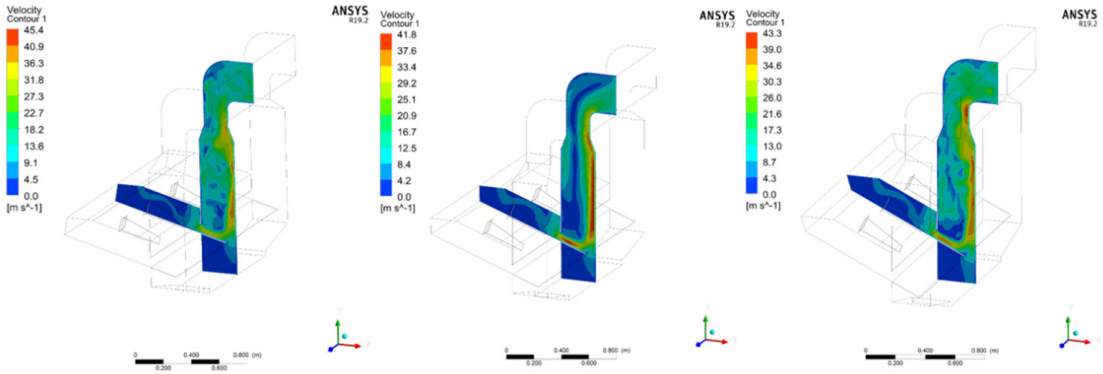

(**a**) (**b**) (**c**)

Figure 6. Cloud map of velocity vector at different angles of 10 m/s. (**a**) 15°. (**b**) 20°. (**c**) 25°.

Figures 3–6 show the three-dimensional streamline diagrams (Figures 3 and 5) and the central cross-sectional velocity vector cloud diagrams (Figures 4 and 6) under different inlet angles at wind speeds of 5 m/s and 10 m/s. The results indicate that when the wind speed is 5 m/s, the three-dimensional streamline diagram is as shown in Figure 3, where the airflow is skewed at an angle of 15° forms vortices at 25°, and the streamlines are relatively stable but have insufficient kinetic energy at 20°. The velocity vector cloud diagram is shown in Figure 4, with an overall lower speed and uneven distribution, and only a local area of the speed meets the requirements for the separation of light impurities. The overall separation effect is poor. When the wind speed is 10 m/s, the three-dimensional streamline diagram is as shown in Figure 5, where, at an angle of 20°, the airflow is relatively stable and diffuses without skewing or vortices, and is evenly distributed. However, at 15°, the airflow is still skewed, and at 25° the vortices are weakened but not eliminated. The velocity vector cloud diagram is shown in Figure 6, with the core area of the speed uniformly distributed between 20 and 25 m/s, suitable for the difference in terminal speed between impurities and wheat grains. At 15°, the speed gradient is large, and at 25° the local speed decays, both of which affect the separation accuracy. In conclusion, the optimal air separation parameters are an inlet speed of 10 m/s and an inlet angle of 20°.

The main reason for the above-mentioned differences in the flow field distribution lies in the direct influence of the intake angle on the boundary conditions of the airflow and the velocity vectors. When the intake angle is 15°, the airflow deflects upwards and impacts the top wall of the cleaning chamber prematurely, resulting in a reflected airflow that exerts downward pressure, thereby weakening the horizontal transport capacity of the airflow for light impurities. When the angle increases to 25°, the airflow axis deviates downward from the main cleaning area, and at the sudden change in the flow channel cross-section it is prone to cause boundary layer separation, resulting in large-scale vortices that lead to a significant dissipation of the airflow energy. In contrast, the velocity vector decomposition at an intake angle of 20° is more reasonable: its horizontal component provides sufficient transport drag force, while the vertical component is precisely between the terminal velocities of light impurities and wheat grains. This flow field structure not only maintains the smooth diffusion of the airflow within the separation chamber but also meets the dynamic conditions for efficient material separation.

4. Fluid–Structure Coupling Simulation Analysis and Optimization of the Cleaning Device

4.1. Parameter Setting

From the wheat grain samples collected during the preliminary research phase, a random sample of 100 grains was measured and averaged. The digital vernier calliper employed had a precision of 0.01 mm. Following measurement and calculation, the wheat kernel dimensions were determined to be 6.6 mm in length, 2.93 mm in width, and 2.89 mm in height (thickness). Referencing the measured dimensions of wheat grains, straw, and other impurities, spherical particles were adopted as the fundamental unit. By adjusting the spatial coordinates of different particles and stacking them, an approximate simulation of the actual material shape was achieved. Specifically, the wheat kernel model comprises five spheres of varying diameters assembled as depicted in Figure 7a, whilst the short stalk model consists of twenty-one spheres of identical diameter as shown in Figure 7b.

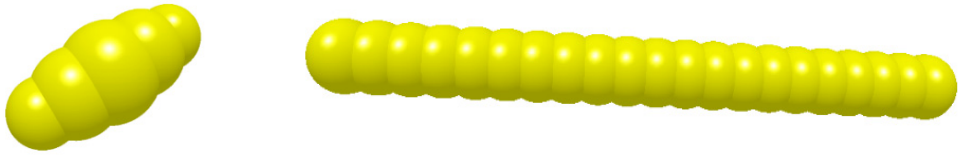

(**a**) (**b**)

Figure 7. Particle-filling 3D models. (**a**) Wheat grain model; (**b**) Short stem model.

The materials contained within the cleaning apparatus comprise wheat grains, short straws, and impurities. The physical parameters of these materials were determined through experimental and literature-based research [5], as detailed in Table 3.

Table 3. Mixture composition table.

Material	Poisson's Ratio	Shear Modulus (MPa)	Density (kg/m^3)
Grain	0.3	2.6	1350
Short stalks	0.4	1	104
Cleaning chamber	0.3	7800	7800

Referencing the classical parameter ranges for the discrete element simulation of granular agricultural materials [20], and incorporating the pre-simulation results of this study, the recovery coefficient, static friction coefficient, and rolling friction coefficient were determined. The specific parameters are shown in Table 4. Specifically, the static friction coefficient between the wheat grains and the vibrating screen was set at 0.58, slightly higher than the inter-particle friction coefficient to ensure effective grain movement. The rolling friction coefficient between short stalks was aligned with that of wheat grains to simulate the readily rolling behaviour of lightweight impurities on the screen surface.

Table 4. Interparticle interaction parameters.

	Restoration Coefficient	Static Friction Coefficient	Dynamic Friction Coefficient
Wheat–Wheat	0.2	1	0.01
Wheat–Short stalks	0.3	0.5	0.01
Wheat–Vibrating screen	0.5	0.58	0.01
Short stalks–Short stalks	0.22	0.5	0.01
Short stalks–Vibrating screen	0.3	0.36	0.01

4.2. Coupled Simulation Configuration

The CFD component utilizes ANSYS Fluent, while the DEM component employs EDEM software 2022 Version, with coupling achieved through a compiled interface. The particle generation zone is defined as a 1400 mm × 500 mm rectangular space within the cleaning chamber, dynamically generating 2000 wheat grains, 500 stalks, and 150 impurities per second. The vibration parameters of the vibrating screen were determined based on prior simulation results [21]: a vibration frequency of 8 Hz, amplitude of 25 mm, and vibration direction angle of 20°. The total simulation duration was 8 s. For comparative analysis, two operating conditions were established: with airflow and without airflow.

In the CFD-DEM-coupled calculation, the inter-particle forces are modelled using the Gidaspow drag force model and the Saffman lift force model, while particle collisions are simulated using the Hertz–Mindlin (no slip) and standard rolling friction models. The DEM time step is set to 24% of the Rayleigh time step, and the data coupling interaction interval is 100 DEM time steps. Additionally, the particle generation rate, converted to mass feed rate, is approximately 250–300 kg/h, which matches the actual processing capacity of typical laboratory-level sorting devices.

4.3. Material Flow Characteristics

Under optimal air separation and vibration parameters, CFD-DEM coupled simulations reveal that material undergoes a sequence of falling, dispersion, separation, and collection within the cleaning chamber, as illustrated in Figure 8. At 0.2 s (Figure 8a), material descends from the generation zone onto the screen surface. The flow field within the cleaning chamber begins to establish, with particle clusters transported forward by the screen's motion. At 1 s, as depicted in Figure 8b, the material gradually disperses under the combined effects of screen vibration and airflow. At 2 s, as shown in Figure 8c, some wheat grains pass through the screen apertures into the collection bin, while short straw begins to be entrained by the airflow. At 8 s, as illustrated in Figure 8d, the majority of wheat grains are collected, while short straw is either blown out of the cleaning chamber by the airflow or remains retained on the screen surface.

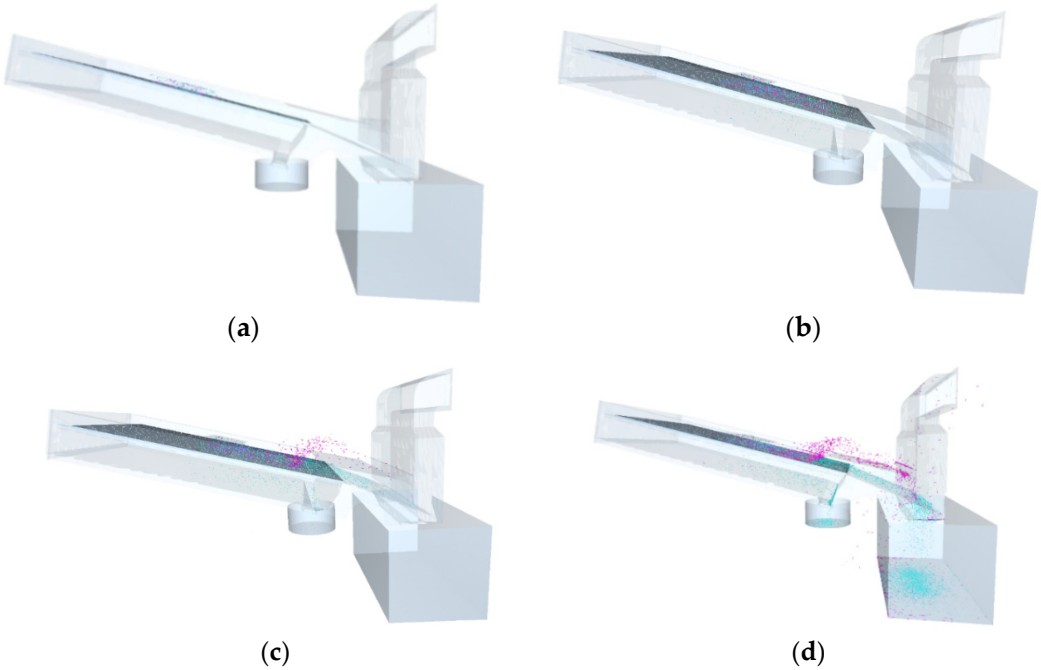

Figure 8. Simulation time chart of the sorting room: (**a**) t = 0.2 s; (**b**) t = 1 s; (**c**) t = 2 s; and (**d**) t = 8.

4.4. Comparison of Wind and Windless Conditions

Analysis comparing the movement trajectories of material within the cleaning chamber under winded and windless conditions reveals that, as shown in Figure 9, the trajectories of material at the front end of the screen are largely consistent. However, significant differences exist in the rear section of the screen. In the aerated condition, lighter impurities are visibly lifted by the airflow (yellow trajectories). The wheat collection device in the aerated condition contains fewer yellow trajectories than in the non-aerated condition.

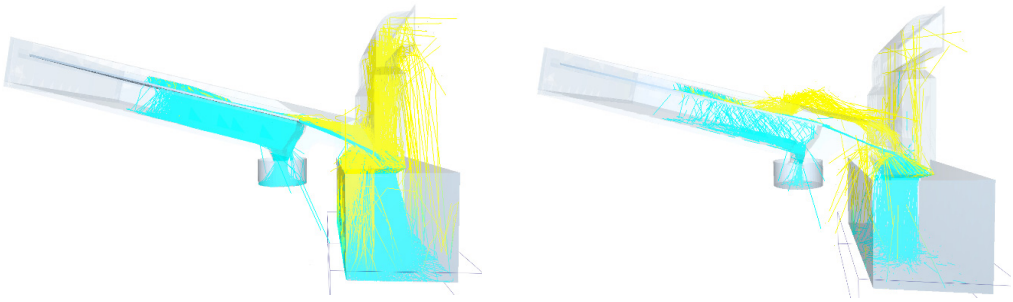

(**a**) (**b**)

Figure 9. The trajectory of the material inside the cleaning chamber with or without the wind field: (**a**) motion trajectory under windless conditions; (**b**) motion trajectory under windy conditions.

The quantity of impurities within the wheat collection apparatus was processed as illustrated in Figure 10. The results indicate that, under windless conditions, impurities could not be effectively separated, with 573 impurities accumulating within the collection box. Under wind conditions, airflow lifted the lightweight impurities, resulting in 265 impurities entering the wheat collection box; this represents a 53.8% reduction in impurity quantity compared to windless conditions. This demonstrates that the optimized equipment, incorporating a high-pressure blower, significantly enhances the cleaning efficiency.

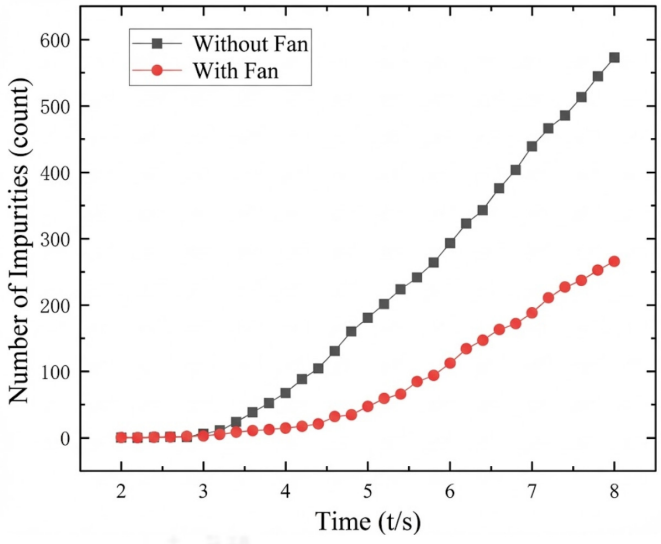

Figure 10. Number of impurities in the square collection devic.

The improvement of the above separation effect can be explained by particle dynamics and the fluid–solid coupling mechanism. In the tail area of the screen, the main airflow undergoes energy attenuation due to the resistance along the way, causing some short stems with greater gravity and light impurities to easily detach from the airflow and undergo sedimentation. The high-pressure fan added at the bottom constructed a vertical upward

compensatory airflow field at the screen tail. Since the terminal speed of short stems and other light impurities (2.0–6.0 m/s) is significantly lower than that of wheat grains (9.5–10.3 m/s), the lift provided by this compensatory airflow is sufficient to overcome the impurity gravity and allow them to re-suspend, be captured by the main airflow, and be sent to the dust collection box again. At the same time, this wind speed is much lower than the terminal speed of wheat grains, so it will not interfere with their original dispersion trajectory. This local flow field compensation mechanism, by selectively applying airflow lift, effectively changes the movement path of the sedimented impurities and is the main reason for the significant reduction in the impurity content at the screen tail.

5. Operational Testing of the Wheat Cleaning Device

5.1. Whole-Machine Experiment

Through conducting working tests on the complete machine of the wheat cleaning device, based on the simulation data mentioned earlier, the inlet wind speed was set at 10 m/s, the inlet angle was 20°, the screen surface inclination angle was 3°, the vibration direction angle was 20°, the vibration frequency was 8 Hz, and the vibration amplitude was 25 mm. The parameters of each part of the wheat cleaning equipment were adjusted. In the verification of the experiment, this study adopted the control variable method and precisely controlled the inlet wind speed through equipment such as frequency converters to strictly match the boundary conditions set in the simulation. Due to the opaque metal structure of the cleaning chamber and the high concentration of the gas–solid two-phase flow inside, directly using optical or wind speed instruments to measure the internal flow field and particle trajectories encountered physical interference and practical difficulties. Therefore, the determination of the wheat impurity rate and the loss rate of the grains were used as the test indicators. The complete machine working test of the wheat cleaning device was carried out, and the test device is shown in Figure 11. In total, 600 kg of wheat harvested by the combine harvester was prepared. The preparation conditions before the test were consistent with those of the previous test, and the test was repeated five times to eliminate the errors and randomness of the test. The test results are shown in Table 5. The average impurity rate of the five tests was 1.722%, and the loss rate was 0.622%. Compared with the existing cleaning equipment in Yunlong, the impurity rate was reduced by 0.23% and the loss rate was reduced by 0.12%, achieving the design optimization of the wheat cleaning device. The optimization of the complete machine test results of the wheat cleaning device also indicates the feasibility of the previous simulation and simulation experiments.

(**a**) (**b**)

Figure 11. The overall working test site of the cleaning device: (**a**) site photograph of operational testing; (**b**) site photograph of operational testing.

Table 5. Overall work performance test of scavenging equipment.

Number of Tests	Impurity Content (%)	Loss Rate (%)
1	1.65	0.64
2	1.74	0.62
3	1.73	0.58
4	1.87	0.59
5	1.62	0.68

5.2. Discussion of Results and Comparative Analysis

Compared with previous studies and existing cleaning equipment, the proposed optimization scheme in this research demonstrates better applicability in terms of its comprehensive cleaning performance. Due to the limitations of the airflow field distribution and the effect of a single physical field, the annual loss rate of existing wheat cleaning equipment typically fluctuates between 1.5% and 3%, and the impurity content often exceeds the safety standard for storage ($\leq$2%). Previously, Wang Peng et al. [10] effectively reduced the wheat loss rate to 0.89% by the CFD reconstruction of the cleaning flow field. However, traditional methods relying on the optimization of a single airflow parameter often face the constraint of being unable to balance the impurity content and loss rate. In contrast, this research, based on determining appropriate flow field parameters to ensure uniform coverage of the main airflow, further utilized the CFD-DEM bidirectional coupling technology to analyze the local deposition of impurities at the tail of the screen due to the attenuation of airflow energy. Based on this fluid–solid coupling mechanism feedback, this research proposed a structural compensation strategy of installing a tail high-pressure fan on the basis of parameter optimization. The repeated test results of the entire machine show that this combined strategy, while ensuring that the impurity content meets the national storage standards, reduces the grain loss rate to 0.622%. This test data is lower than the industry average loss level and is superior to the optimization results in some literature. This indicates that the comprehensive multi-parameter flow field optimization and the structural improvement based on micro-motion feedback can effectively alleviate the engineering problem of the difficulty in simultaneously reducing the impurity content and loss rate during cleaning.

6. Conclusions

In this study, the airflow parameters were optimized via CFD simulation, and the fluid–structure interaction mechanism of the wheat cleaning device was analyzed through the CFD-DEM coupling simulation, followed by structural improvement. These measures effectively addressed the problems of a high impurity content rate and high grain loss rate. The main conclusions are as follows:

(1) The CFD simulations of the internal airflow field within the wheat cleaning apparatus demonstrate that both the inlet air velocity and inlet angle exert a significant influence on the air separation efficacy. The optimal air separation parameters are determined to be an inlet air velocity of 10 m/s and an inlet angle of 20°, under which conditions of airflow distribution are uniform and the impurity separation efficiency is maximized.

(2) The structural optimization of the cleaning apparatus through the installation of a high-pressure blower effectively enhanced cleaning performance. Coupled CFD-DEM simulation results indicate that under aerated conditions, the impurity count within the wheat collection bin was 265 particles, representing a 53.7% reduction compared to non-aerated conditions. The research findings demonstrate that the CFD-DEM coupled method can effectively simulate the internal flow field and fluid–

structure interaction within the wheat cleaning apparatus, providing a scientific basis for parameter optimization and structural improvements.

(3) The engineering applicability of the simulation-optimized and structurally improved design was further validated through full-scale operational trials. Five repeated trials were conducted using the optimal airflow parameters and vibration parameters (vibration frequency 8 Hz, amplitude 25 mm, and vibration direction angle 20°). The results showed an average impurity content of 1.722% and an average loss rate of 0.622%, representing reductions of 0.23% and 0.12% respectively compared to existing cleaning equipment. These figures meet the storage and processing standards for practical production.

Author Contributions: Conceptualization, Y.Q. and L.D.; Methodology, S.Y.; Software, L.Z.; Validation, C.Z.; Formal analysis, Y.Q.; Investigation, L.D.; Data curation, L.Z.; Writing—original draft, J.H. and S.Y.; Writing—review & editing, C.Z.; Visualization, L.D.; Supervision, Y.Q.; Project administration, Y.Q.; Funding acquisition, Y.Q. All authors have read and agreed to the published version of the manuscript.

Funding: Key Technology Research and Industrialization of Multifunctional Intelligent Precision Grain Cleaning Equipment Major Natural Science Project of the Anhui Provincial Department of Education: 2022AH040238. Anhui Provincial Natural Science Foundation General Programme: Research on Multi-Physics Field Coupled Vibration Control of Wind Turbine Blades (2308085ME178). Anhui Province High-Efficiency Collaborative Innovation Project: Research on Key Technologies and Equipment for Intelligent, Efficient Solidification and Moulding of Fertilizer Produced by Pyrolysis Carbonisation of Agricultural and Forestry Waste Materials GXXT-2023-058. Anhui Province Agricultural Material Challenge-Based Project. Weighing Fruit Sorter (311152350024). 2022 Anhui Provincial Collaborative Innovation Project: 'Key Technology Research for Multi-Rod Grain Sampling Equipment Based on Visual Recognition'. GXXT-2022-077. Anhui Higher Education Collaborative Innovation Project: GXXT-2023-022.

Institutional Review Board Statement: Not applicable.

Informed Consent Statement: Not applicable.

Data Availability Statement: The data presented in this study are available on request from the corresponding author.

Conflicts of Interest: Authors Chunyan Zhang and Junrong He were employed by the company Anhui Yunlong Grain Machinery Co., Ltd. The remaining authors declare that the research was conducted in the absence of any commercial or financial relationships that could be construed as a potential conflict of interest.

References

1. Li, Z.; Zhao, J.; Ou, X.; Li, X.; Ding, X.; Wang, Y.; Huang, Z.; Ma, S.; Fan, Y.; Zhang, W. Effects of different fertilizer types and nitrogen levels on nitrogen utilization, yield and quality of weak-gluten wheat. *Sci. Agric. Sin.* **2025**, *58*, 3690–3709.
2. Wang, H.; Li, Y.; Xu, L.; Fu, Y. Analysis and experiment of internal airflow field of cleaning device for ratoon combine harvester. *Trans. Chin. Soc. Agric. Eng.* **2020**, *36*, 84–92.
3. Jiang, T.; Li, H.; Guan, Z.; Mu, S.; Wu, C.; Zhang, M. Design and experiment of material dispersing and guiding device on rape harvesting and cleaning sieve surface. *Trans. Chin. Soc. Agric. Mach.* **2023**, *54*, 146–158.
4. Wang, F.; Li, B.; Zhu, R.; Wang, S.; Liu, Y.; Gao, X.; Yang, X. Design and experiment of air-screen cleaning device for cumin thresher. *Trans. Chin. Soc. Agric. Eng.* **2024**, *40*, 39–50.
5. Orobinsky, V.I.; Gievsky, A.M.; Gulevsky, V.A.; Baskakov, I.V.; Chernyshov, A.V. Obtaining high-quality grain through the use of fractional technology for its cleaning. In *IOP Conference Series: Earth and Environmental Science*; IOP Publishing: Bristol, UK, 2021; Volume 640, p. 022046.
6. Umbarov, I.; Karimov, F.; Karimov, Z.; Bekkamov, M.; Ubaydullayev, A.; Eshkuvatov, E.; Israilova, D. Gravity grain cleaning machine and its importance in grain logistics and sustainable agriculture. In *BIO Web of Conferences*; EDP Sciences: Les Ulis, France, 2024; Volume 105, p. 06016.

7. Li, X.; Du, Y.; Niu, X.; Chi, R.; Mao, E. Structural optimization design and experiment of corn cleaning device. *Trans. Chin. Soc. Agric. Mach.* **2020**, *51*, 233–242.
8. Ueka, Y.; Matsui, M.; Inoue, E.; Mori, K.; Okayasu, T.; Mitsuoka, M. Turbulent Flow Characteristics of the Cleaning Wind in Combine Harvester. *Eng. Agric. Environ. Food* **2012**, *5*, 102–106. [CrossRef]
9. Gebrehiwot, M.G.; de Baerdemaeker, J.; Baelmans, M. Computational and experimental study on effect of a cross-flow opening on the performance of a centrifugal fan in a combine harvester. *Biosyst. Eng.* **2010**, *105*, 247–256. [CrossRef]
10. Peng, W.; Chengqian, J.I.; Chao, W.; Panpan, L.; Zihao, Z. Research status of threshing system for grain combine harvester. *J. Chin. Agric. Mech.* **2023**, *44*, 48–57.
11. Qiang, S. *Numerical Simulation and Optimization Analysis of Flow Field in Cleaning Device of Longitudinal Axial Flow Full-Feed Combine Harvester*; Zhejiang University: Hangzhou, China, 2016.
12. Yang, M.; Hu, Z.; Zhang, Y.; Xu, H.; Gu, F.; Wu, F. Research status and prospect of pneumatic cleaning device for agricultural granular materials. *J. Chin. Agric. Mech.* **2020**, *41*, 121–127. [CrossRef]
13. Wang, F.; Alimu, M.; Zhang, J.; Li, Q.; Xu, L. Design and experiment of combined sieve surface pre-screening cleaning device for corn grain harvester. *Trans. Chin. Soc. Agric. Mach.* **2024**, *55*, 135–147, 166.
14. Pang, J.; Lin, Y.; Wang, S.; Du, Z.; Xie, L.; Chen, X. Vibration analysis and structural optimization of grain cleaning sieve based on VMD. *Trans. Chin. Soc. Agric. Eng.* **2023**, *39*, 1–9.
15. Lei, X.L.; Liao, Y.T.; Liao, Q.X. Simulation of seed motion in seed feeding device with DEM-CFD coupling approach for rapeseed and wheat. *Comput. Electron. Agric.* **2016**, *131*, 29–39. [CrossRef]
16. Chu, K.W.; Wang, B.; Xu, D.L.; Chen, Y.X.; Yu, A.B. CFD-DEM simulation of the gas-solid flow in a cyclone separator. *Chem. Eng. Sci.* **2011**, *66*, 834–847. [CrossRef]
17. Xiao, X.; Li, H.; Wu, C.; Qi, X.; Hu, T. Motion analysis of cleaning process of cylindrical sieve for two early rice varieties based on DEM-CFD. *J. Mach. Des.* **2018**, *35*, 32–37.
18. Zhang, K.; Fan, H.; Sun, B.; Dong, X.; Hu, J.; Li, H. CFD-DEM gas-solid coupling simulation and experimental verification of cleaning device for wheat combine harvester under intercropping mode. *Agric. Res. Arid. Areas* **2019**, *37*, 268–274.
19. Kharitonov, M.K.; Gievsky, A.M.; Orobinsky, V.I.; Chernyshov, A.V.; Baskakov, I.V. Studying the design and operational parameters of the sieve module of the grain cleaning machine. In *IOP Conference Series: Earth and Environmental Science*; IOP Publishing: Bristol, UK, 2020; Volume 488, p. 012021.
20. Xu, B.; Zhang, Y.; Cui, Q.; Ye, S.; Zhao, F. Construction of a discrete element model of buckwheat seeds and calibration of parameters. *INMATEH Agric. Eng.* **2021**, *64*, 175–184. [CrossRef]
21. He, J.; Zhang, C.; Zhang, L.; Qi, P. Modeling of wheat kernels and simulation analysis of vibrating screen based on EDEM. *J. Bengbu Univ.* **2024**, *13*, 35–39.